Morphology and Thermodynamic Behavior of Syndiotactic Polypropylene−Poly(ethylene-*co*-propylene) Block Polymers Prepared by Living Olefin Polymerization

Janne Ruokolainen,[†] Raffaele Mezzenga,[‡] Glenn H. Fredrickson, and Edward J. Kramer*

Mitsubishi Chemical Center for Advanced Materials and the Departments of Materials and Chemical Engineering, University of California, Santa Barbara, California 93106

Phillip D. Hustad[§] and Geoffrey W. Coates*

Department of Chemistry and Chemical Biology, Baker Laboratory, Cornell University, Ithaca, New York 14853

Received March 19, 2004; Revised Manuscript Received October 21, 2004

ABSTRACT: We investigate the morphology and phase behavior of syndiotactic polypropylene-*block*-poly(ethylene-*co*-propylene) (sPP-EPR) and syndiotactic polypropylene-*block*-polyethylene (sPP-PE) block copolymers. Order−disorder transition temperatures of selected sPP-EPR block copolymers, determined by dynamic mechanical spectroscopy (DMS) and confirmed by transmission electron microscopy (TEM), were analyzed using mean field theory to obtain $\chi(T)$, the Flory−Huggins interaction parameter for the sPP/PE pair, as $\chi_{sPP-PE} = 6.2/T - 0.0053$ normalized to a four-carbon repeat unit. Various ordered morphologies were observed by TEM, including cylindrical, lamellar, and hexagonally perforated layer morphologies, the latter being most often observed despite the fact that it is expected to be metastable. The sPP crystallization and melting temperatures, T_c and T_m, determined by differential scanning calorimetry (DSC), show surprisingly little correlation with either block copolymer morphology or the state of block copolymer melt phase (ordered or disordered) but rather increase with decreasing total molecular weight of the block copolymer. Both blocks of the sPP-PE crystallize, but the PE T_c and T_m of an ordered lamellar sPP-PE are significantly higher than those of an ordered sPP-PE consisting of sPP cylinders in a PE matrix.

Introduction

On the basis of the annual production volume, polyolefins are by far the most important class of commodity plastics. The widespread use of polyethylene (PE) and polypropylene (PP) materials is largely due to their excellent mechanical properties, the inexpensive nature of monomers, and their ease of production, manufacturing, and processing.[1] However, polyolefin production has largely been limited to bulk commodity homopolymers and random copolymers due to synthetic restrictions imposed by Ziegler−Natta[2] or metallocene[3−5] polymerization methods. Novel polyolefin chain architectures, such as block copolymers with random ethylene-*co*-propylene blocks and semicrystalline PE or PP blocks, have tremendous potential in various applications since their macroscopic properties can vary from elastomeric to plastic depending on the volume fraction of the poly(ethylene-*co*-propylene) rubbery block. However, such block copolymers have been difficult to synthesize with traditional methods, as chain transfer reactions prohibit sequential monomer addition techniques.[6]

To address the limitations of traditional catalyst systems with respect to block copolymer synthesis, Coates and Waymouth developed a strategy for synthesis of stereoblock polypropylenes using an unbridged bis(indenyl) metallocene catalyst system.[7] By controlling the polymerization conditions, the catalyst was tuned to oscillate between isospecific and aspecific states on the time scale of chain propagation, thus producing stereoblock copolymers with multiple isotactic and atactic segments. The combination of crystalline and amorphous domains in one polymer chain resulted in materials with good mechanical properties, including high ultimate elongations and low tensile sets. However, commercial applications of these thermoplastic elastomers were limited due to the relatively high glass transition temperature of the atactic polypropylene domains ($T_g \approx 0$ °C).

Polymerization process techniques have also been utilized to prepare polyolefin block copolymers. For example, Terano and co-workers reported the synthesis of isotactic polypropylene-*block*-poly(ethylene-*co*-propylene) (iPP-EPR) block copolymers using a short period stopped flow polymerization technique.[8] With this method, a "quasiliving polymerization" was achieved by quenching the polymerization after a very short length of time (up to 0.2 s), thus avoiding undesired termination reactions by halting chain growth before a chain transfer event could take place. However, the short residence times necessary for stopped flow methods make the controlled synthesis of these materials very difficult.

Recently, a number of catalyst systems have been discovered to polymerize olefin monomers in a living or controlled fashion.[9] These catalysts, largely based on

[†] Current address: Department of Engineering Physics, Optics, and Molecular Materials, Helsinki University of Technology, P.O. Box 2200, FIN-02015 HUT, Finland.

[‡] Current address: Nestlé Research Center, Vers-Chez-Les-Blanc, 1000 Lausanne 26, Switzerland.

[§] Current address: Polyolefins and Elastomers R&D, The Dow Chemical Company, 2301 N. Brazosport Blvd., B-3814, Freeport, TX 77541.

* Corresponding authors. E-mail: edkramer@mrl.ucsb.edu or gc39@cornell.edu.

10.1021/ma0494479 CCC: $30.25
Published on Web 01/05/2005

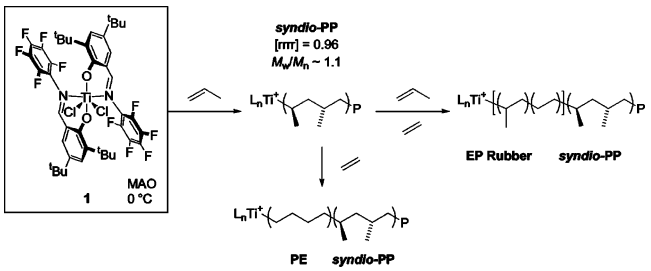

Figure 1. Synthesis of *syndio*-polypropylene-*block*-poly(ethylene-*co*-propylene) and *syndio*-polypropylene-*block*-polyethylene diblock copolymers with the bis(phenoxyimine)-based catalyst system **1**/MAO.

non-metallocene ligand architectures, have enabled the synthesis of a wide range of polyolefin block copolymers. For thermoplastic elastomer applications, the potential of these new catalyst systems lies in their ability to give polymers with high glass or melting transitions from simple olefin monomers. Coates and co-workers have reported a catalyst system capable of synthesizing polyolefin block copolymers with high melting stereoregular domains from ethylene and propylene monomers.[10] They discovered that the fluorinated bis(phenoxyimine)-based titanium catalyst system **1**/MAO gave highly syndiotactic polypropylenes (sPP, ([rrrr] = 0.96) with very narrow molecular weight distributions ($M_w/M_n \sim 1.1$) (Figure 1).[10,11] Block copolymers were also accessible with this system via sequential monomer addition, providing access to a variety of interesting polyolefin copolymer architectures (Figure 1).[10,12,13] Copolymers containing both crystalline sPP and amorphous EPR domains are of particular commercial interest due to the high upper melting temperature of the sPP (T_m > 140 °C) and the low glass transition temperature (T_g < −40 °C) of the EPR domain. Fujita and co-workers have independently reported the synthesis of ethylene/propylene block copolymers using a similar catalyst system.[14,15] In addition, isotactic polypropylene-*block*-polyethylene (iPP-PE) block copolymers have been synthesized[16] using a structurally related phenoxyamine Zr-based catalyst.[17]

Polyolefin block copolymers or binary blends are an ideal system for studying polymer thermodynamics. Different polyolefins, e.g. PE and PP, are chemically very similar but can exhibit significant differences in mixing behavior with respect to molecular architecture. Therefore, strong interactions, such as hydrogen bonding or polar interactions that complicate the theoretical modeling, can be neglected in these systems; the only type of contribution to be accounted for is the dispersion interaction. Fluctuation effects on order−disorder transition temperatures are also minimal because polyolefin block copolymers are weakly segregated up to relatively high molecular weights.

Earlier work on semicrystalline−rubbery block copolymer thermodynamics largely focused on systems where polyethylene is the crystalline block with various rubbery blocks, including atactic polypropylene (PE-aPP),[18] head-to-head polypropylene (PE-hhPP),[19−21] poly(ethylene-*co*-propylene) (PE-PEP), or poly(ethyl ethylene) (PE-PEE).[22−31] Research on these systems mainly focused on morphology and phase behavior,[22−27] crystallization kinetics,[28,29] and the dynamics of structure development during crystallization.[30,31] The advantage of using polyethylene as a crystallizable block is the fact that block copolymers containing polyethylene and atactic polyolefins can be obtained indirectly by the hydrogenation of polydienes synthesized by anionic polymerization techniques. However, stereoregular polypropylene block copolymers cannot be synthesized with this methodology.

In this paper, we report the morphology and phase behavior of syndiotactic polypropylene-*block*-poly(ethylene-*co*-propylene) (sPP-EPR) and syndiotactic polypropylene-*block*-polyethylene (sPP-PE) block copolymers made by living olefin polymerization. The temperature-dependent Flory−Huggins interaction parameter between PE and sPP units is determined from order−disorder transition temperatures using mean field theory. Crystallization and melting of sPP and PE blocks are studied using differential scanning calorimetry (DSC).

Experimental Section

General Considerations. All manipulations of air- and/or water-sensitive compounds were carried out under dry nitrogen using a Braun Labmaster drybox or standard Schlenk line techniques. Copolymer compositions were determined by ^{13}C NMR spectra of the polymers, which were recorded on a Varian VXR-400 (100 MHz) spectrometer and referenced vs residual nondeuterated solvent shifts. The polymer samples were dissolved in 1,1,2,2-tetrachloroethane-d_2 (TCE) in a 5 mm o.d. tube by heating to 120 °C in an oil bath. An inverse gated decoupling sequence was employed with a 30° pulse width over a 160 ppm spectral width at a 2.0 s acquisition time to minimize NOE and allow for quantitative analysis.

Molecular weights (M_w and M_n) and polydispersities (M_w/M_n) were determined by high-temperature gel permeation chromatography (GPC). All analyses were performed with a Waters Alliance 2000 liquid chromatograph equipped with a Waters DRI detector and a Jordi styrene−divinylbenzene linear mixed-bed column. The GPC columns were eluted with 1,2,4-trichlorobenzene (TCB) containing 0.1 wt % Irganox 1010 at 140 °C at 1.0 mL/min and were calibrated using 23 monodisperse polystyrene standards. Polymer samples were typically placed in a 140 °C oven for 24 h to eliminate supramolecular aggregates prior to molecular weight measurements.

Materials. Toluene was distilled from sodium benzophenone ketyl under nitrogen. Propylene (Matheson, polymer grade) was purified through a mixed bed column (R&D Separations, BOT-4). Methylaluminoxane (Akzo Nobel, PMAO-IP, 12.9 wt % Al in toluene) was concentrated in vacuo to dryness (10^{-3} mmHg) at 40 °C for 18 h to remove residual trimethylaluminum, providing a solid white powder. Complex **1** was prepared as described in the literature.[10] All other chemicals were commercially available and used as received.

Polymerizations. *General Synthetic Procedure for Syndio-PP-block*-EPR. A 6 oz Lab-Crest pressure reaction vessel equipped with a magnetic stir bar was first conditioned under dynamic vacuum and high temperature and then charged with PMAO (0.87 g, 15 mmol) and toluene (100 mL). An IKA magnetic stirrer was positioned, and the stirring rate was set at 8. The reactor was cooled to 0 °C, and the atmosphere was exchanged with propylene gas three times, and then saturated under pressure (30 psi). A solution of titanium complex **1** (0.092 g, 0.10 mmol) in toluene (4 mL) was then added to the reactor via gastight syringe to initiate the polymerization. After the prescribed time, a 5 mL sample was removed via cannula, the reactor was vented (3 min) to a residual pressure of ca. 3 psi, and ethylene (40 psi) was introduced into the reactor. After the desired additional polymerization time, the reaction was quenched by injection of methanol/HCl (5 mL, 10 vol % HCl). After venting the reactor, the polymer was precipitated in copious methanol/HCl, filtered, washed with methanol, and dried in vacuo to constant weight.

General Synthetic Procedure for Syndio-PP-block-PE. A 6 oz Lab-Crest pressure reaction vessel equipped with a mag-

netic stir bar was first conditioned under dynamic vacuum and high temperature and then charged with PMAO (0.17 g, 2.9 mmol) and toluene (100 mL). An IKA magnetic stirrer was positioned, and the stirring rate was set at 8. The reactor was cooled to 0 °C, and the atmosphere was exchanged with propylene gas three times, and then saturated under pressure (30 psi). A solution of titanium complex **1** (0.009 g, 0.01 mmol) in toluene (4 mL) was then added to the reactor via gastight syringe to initiate the polymerization. After the prescribed time, the reactor was vented until the pressure reached ca. 2 psi. The ice bath was then removed, and the liquid propylene was removed in vacuo. When the solvent had returned to its original level, indicating complete removal of propylene, ethylene (3 psi) was introduced into the reactor. After the desired additional polymerization time, the reaction was quenched by injection of methanol/HCl (5 mL, 10 vol % HCl). After venting the reactor, the polymer was precipitated in copious methanol/HCl, filtered, washed with methanol, and dried in vacuo to constant weight.

Transmission Electron Microscopy (TEM). All samples for TEM were annealed in the melt for a total of 8 days—the first 4 days at 200 °C to erase any previous thermal history and then an additional 4 days at a final temperature 160 °C. High-vacuum ovens ($<10^{-7}$ mbar) were used to prevent degradation by oxidation. Melt morphology was preserved by quickly quenching the samples after annealing. Fast cooling was achieved by immersing samples into liquid propane.

TEM images of quenched samples were recorded at 200 kV with a JEOL 2000FX instrument. The contrast for the morphological characterization was achieved by a sample preparation technique that relies on different rates of diffusion of a RuO_4 stain into the amorphous and semicrystalline regions.[32] First, the sample surface was cut at −170 °C to make a smooth surface for the stain to penetrate into the sample. The samples were then stained in a vapor of a 0.5% RuO_4 stabilized aqueous solution (Electron Microscopy Science) for a period of between 5 and 7 days. The stained sample was microtomed using a Leica Ultracut UCT ultramicrotome with a diamond knife at room temperature, and 80 nm thick sections were collected on 600 mesh hexagonal grids.

Differential Scanning Calorimetry (DSC). Thermal analysis measurements were performed using a TA Instruments 2920 calorimeter. The DSC measurements reported in the present work are recorded during the second heating/cooling cycle with the rate of 5 °C/min. This procedure ensures that previous thermal history is erased and provides comparable conditions for all samples. Each sample for DSC was approximately 5 mg.

Dynamic Mechanical Analysis. The dynamic storage G' and loss moduli G'' were measured using a Rheometrics ARES rheometer in oscillation mode using a 25 mm diameter cone-and-plate geometry. Measurements were collected over a frequency range from 0.1 to 100 rad/s at temperatures between 100 and 350 °C. In a few cases, the frequency range was extended down to 0.01 rad/s, although the very low torque at low frequencies and high temperatures and the very long measurement times limited the study to the 0.1−100 rad/s range for the majority of the samples. A nitrogen atmosphere was used to prevent sample degradation. The strain amplitude range of 1−10% used was within the linear viscoelastic range of all the materials considered.

Results and Discussion

According to mean-field theory, for a monodisperse symmetric AB diblock copolymer, the order−disorder transition (ODT) occurs at a fixed interaction strength, $\chi N = 10.5$, where χ is the Flory−Huggins interaction parameter and N is the total number of segments. Symmetric block copolymers have a composition $f_A = 0.5$ and equal statistical segment lengths, $b_A = b_B$. For polyolefin systems, the molar volume of a polymer with N segments is commonly normalized with respect to the reference volume of 71.1 cm^3/mol, which is the molar density of most four-carbon polyolefin segments at 140 °C and corresponds to a volume of 118 $Å^3$ at a molecular level.[33,34] In addition to these three parameters (χ, N, and f_A), which have the greatest influence on the block copolymer phase behavior, the statistical segment lengths and volumes define a fourth parameter, which is called the conformational asymmetry parameter. It describes the differences between how each of the two blocks fill their respective domains in a microphase-separated melt. In general, the statistical segment length is different for each polymer, and even small changes in chain configuration can have a large effect on the statistical segment length and therefore also on other physical properties. For example, the statistical segment length for syndiotactic polypropylene, sPP, in a melt at 180 °C is 7.6−8.1 Å,[35] which is significantly larger than the corresponding value of 5.6 Å for isotactic or atactic forms of polypropylene.[36] However, the statistical segment length for polyethylene at 180 °C is also approximately 8 Å.[26] Therefore, conformational asymmetry for sPP-PE block copolymers is negligible. Since our poly(ethylene-*co*-propylene) (EPR) block contains typically 70−80% polyethylene, the EPR block statistical segment length is also expected to be very similar to that of PE and sPP. Therefore, the total number of segments N for this system can be simply calculated by dividing the total molecular weight by 56, which is the molar mass of the four-carbon segment.

Temperature Dependence of the Flory−Huggins Interaction Parameter $\chi(T)$. The temperature dependence of $\chi(T)$ typically has the form $\chi(T) = A/T - B$, where T is absolute temperature and A and B are constants that are proportional to the nonideal enthalpy and entropy of mixing, respectively. Several methods have been utilized to determine $\chi(T)$. For example, one method consists of applying the random phase approximation to the results from scattering experiments using either binary homopolymer blends or diblock copolymers in a disordered melt state. Measurements of temperature-dependent segregation of short A−B diblock copolymers to an interface between A and B homopolymers have also been used to determine $\chi(T)$.[37] The method adopted in this study is to determine the $\chi(T)$ from the diblock copolymer order−disorder transition by applying mean-field theory. This method requires measuring the order−disorder transition temperatures, T_{ODT}, for several block copolymer samples that have similar compositions but different total molecular weights.

Dynamic mechanical spectroscopy has been shown to be a very efficient tool to determine the T_{ODT} for block copolymers.[38] One procedure to determine T_{ODT} from rheological data is to use isothermal frequency scans at different temperatures. For symmetric A−B diblock copolymers with lamellar order, the dynamic storage modulus $G'(\omega)$ scales as $\sim\omega^{0.5}$ as $\omega \to 0$ below the order−disorder transition temperature. Above the ODT $G'(\omega)$ scales as $\sim\omega^{2.0}$ as $\omega \to 0$ just as for homopolymer melts.[38,39] However, the measurement of G' at fixed frequency during slow heating is a more convenient method to determine T_{ODT}. When plotted as a function of temperature, the low-frequency dynamic storage modulus G' often drops rapidly above T_{ODT}. If however the order-to-disorder transformation is sluggish due to the high molecular weight and high entanglement density of the block copolymer, the ODT may not be so easily discerned. Han and co-workers proposed another

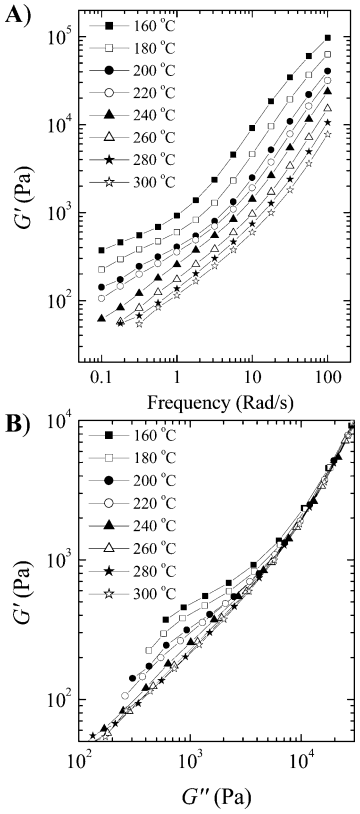

Figure 2. (A) Frequency scans for different constant temperatures of the dynamic storage modulus G' for sample PP58.173EPR measured during heating from 160 to 300 °C with an increment of 20 °C between scans and (B) plot of log $G'(\omega)$ vs log $G''(\omega)$ at various temperatures. The order−disorder transition is assigned to the temperature above which the curves become independent of temperature.

method utilizing plots of log $G'(\omega)$ vs log $G''(\omega)$.[40,41] In their approach, the T_{ODT} corresponds to the temperature at which log(G') vs log(G'') plots become independent of temperature during heating from the microphase-separated state. While Rosedale and Bates[42] showed that this method can produce an overestimate of the true ODT due to the effects of fluctuations on G' and G'', we find that it produces the most reliable results for our sPP-EPR block copolymers.

Figure 2A shows a plot of G' vs ω for an sPP-EPR block copolymer sample at various temperatures. At the lowest temperatures and frequencies, $G'(\omega)$ scales as $\omega^{0.5}$, which corresponds to the typical behavior for a microphase-separated diblock copolymer melt below the order−disorder transition. At higher temperatures, experimental data show an increase of the low-frequency $G'(\omega)$ scaling exponent, although this remains below the theoretical value of 2 expected for the disordered block copolymer. DMS measurements at constant frequency (ω = 0.5 rad/s) as a function of temperature were performed, and again, no sharp changes in G' vs temperature were observed during the slow heating or cooling cycles. However, a plot of log(G') vs log(G'') becomes independent of temperature above 260 °C as seen in Figure 2B. This behavior indicates that an order−disorder transition temperature (T_{ODT}) is between 240 and 260 °C for this block copolymer.

All order−disorder transition temperatures in this study were thus determined using log(G') vs log(G'') plots. All experiments were performed at an average heating or cooling rate of 0.5−1 °C/min (an increment of 5−10 °C between the scans), and the data collected during cooling and heating were identical. Order−disorder transition temperatures obtained from the rheological data were compared with transmission electron microscopy observations after rapid quenching of the samples from 160 °C, and good agreement was found between the two techniques. In particular, all samples designated disordered at 160 °C from rheological data also appeared as disordered in the TEM micrographs, while samples which displayed a T_{ODT} higher than 160 °C by rheology appeared as microphase separated in TEM.

A possible reason a scaling exponent of 2 is never achieved for the highly entangled, disordered sPP-EPR block copolymer melts in our experiments is that the frequencies investigated were not sufficiently low for these systems. A few samples were examined at constant temperature and frequency down to 0.01 rad/s. Unfortunately, the long duration of data acquisition necessary at these low frequencies (a few hours) meant that some degradation of the block copolymer was observed at the high temperatures despite the protective nitrogen atmosphere surrounding the sample. Furthermore, at these low frequencies, the torque developed by the system is below the sensitivity of our rheometer load cell. Therefore, we conclude that combining the log(G') vs log(G'') plot evidence with TEM morphological characterization gives the best estimate of T_{ODT} in all the polyolefin block copolymers studied.

Table 1. Syndiotactic Polypropylene-*block*-poly(ethylene-*co*-propylene) and Syndiotactic Polypropylene-*block*-polyethylene Diblock Copolymers Prepared with the Bis(phenoxyimine) Catalyst System

sample[a]	M_n(PP)[b] (g/mol)	M_n(total)[b] (g/mol)	M_w/M_n[b]	F_e[c] (EPR)	wt % sPP[d]
PP10.380EPR	36 000	380 000	1.19	0.86	9.5
PP11.570EPR	60 000	570 000	1.23	0.80	10.5
PP14.256EPR	36 000	256 000	1.13	0.84	14.1
PP28.214EPR	60 000	214 000	1.13	0.80	28.0
PP35.130EPR	44 800	130 000	1.18	0.77	34.5
PP39.91EPR	35 400	91 000	1.16	0.80	38.9
PP40.243EPR	97 800	243 000	1.31	0.72	40.2
PP43.192EPR	82 200	192 000	1.22	0.79	42.8
PP43.74EPR	32 300	74 400	1.19	0.73	43.4
PP47.212EPR	99 700	212 000	1.26	0.77	47.0
PP49.150EPR	73 800	150 000	1.27	0.70	49.2
PP51.191EPR	98 000	191 000	1.29	0.71	51.3
PP52.168EPR	87 600	168 000	1.28	0.71	52.1
PP52.152EPR	79 600	152 000	1.21	0.75	52.4
PP57.175EPR	99 800	175 000	1.28	0.81	57.0
PP58.173EPR	101 000	173 000	1.27	0.74	58.4
PP59.212EPR	124 000	212 000	1.22	0.75	58.5
PP60.74EPR	44 500	73 600	1.14	0.70	60.4
PP61.116EPR	70 200	116 000	1.18	0.70	60.5
PP71.232EPR	164 000	232 000	1.34	0.63	70.7
PP73.117EPR	85 000	117 000	1.15	0.91	72.7
PP28.350PE	98 000	350 000	1.15	1.0	28.0
PP37.192PE	71 400	192 000	1.28	1.0	37.2
PP41.327PE	134 000	327 000	1.17	1.0	41.0

[a] Sample notation is as follows: the first two letters indicate the first block (PP = syndiotactic polypropylene), the first number is the weight percentage of the syndiotactic PP block, the second number after the period is the total molecular weight in kg/mol, and the letters at the end indicate the second block, which is either poly(ethylene-*co*-propylene) (EPR) or polyethylene (PE). [b] Determined by GPC relative to polystyrene standards. [c] Determined from the ^{13}C NMR spectra. [d] Determined from M_n(PP) and M_n(total) such that wt % sPP = M_n(PP)/M_n(total).

Table 2. Syndiotactic Polypropylene-*block*-poly(ethylene-*co*-propylene) Samples That Were Used To Determine the Temperature Dependence of $\chi(T)$

sample[a]	M_n(total)[b] (g/mol)	N[c]	F_e[d] (EPR)	$(F_e)^2N$	f_{sPP}[e]	T_{ODT} (°C)
PP60.74EPR	73 600	1314	0.70	644	0.60	<110
PP61.116EPR	116 000	2071	0.70	1015	0.61	115
PP58.173EPR	173 000	3089	0.74	1692	0.58	250
PP57.175EPR	175 000	3125	0.81	2050	0.57	305
PP59.212EPR	212 000	3786	0.75	2129	0.59	>300

[a] Sample notation is as follows: the first two letters indicate the first block (PP = syndiotactic polypropylene), the first number is the weight percentage of the syndiotactic PP block, the second number after the period is the total molecular weight in kg/mol, and the letters at the end indicate the second block, which is either poly(ethylene-*co*-propylene) (EPR) or polyethylene (PE). [b] Determined by GPC relative to polystyrene standards. [c] Calculated from the M_n such that $N = M_n/56$. [d] Determined from the ^{13}C NMR spectra. [e] Estimated from M_n(PP) and M_n(total) such that $f_{sPP} = M_n(PP)/M_n(total)$.

Five of the sPP-EPR samples reported in Table 2 had nearly the same composition ($f_{sPP} = 0.57-0.6$) and similar EPR block ethylene fractions ($F_e = 0.7-0.8$), differing only in their respective molecular weights. Therefore, these samples constitute an ideal set for extracting the temperature dependence of the Flory–Huggins interaction parameter. At $f_{sPP} = 0.6$, the calculated mean-field value for χN at the ODT is slightly higher than 10.5, i.e., $\chi N \approx 10.85$. Since the poly(ethylene-*co*-propylene) block is a random copolymer of ethylene and propylene, we can further approximate the effective $\chi_{sPP-EPR}$ for sPP-EPR to be simply given by $\chi_{sPP-EPR} \approx (F_e)^2\chi_{sPP-PE}$,[43-45] where the χ_{sPP-PE} is the Flory–Huggins parameter between sPP and PE segments. Therefore, at the T_{ODT}, $\chi_{sPP-EPR}$ will be given by

$$\chi_{sPP-EPR} \approx 10.85/(N(F_e)^2) \quad (1)$$

As can be observed in Figure 3, a plot of $\chi(T)$ vs $1/T$ yields a straight line, and a linear least-squares fit to the data gives the following values for $\chi(T) = A/T - B$:

$$\chi_{sPP-PE} = 6.2/T - 0.0053 \quad (2)$$

These measured χ values for sPP/PE are very similar to those of other related polyolefin block copolymer systems. For example, the magnitude of the Flory–Huggins parameter for the sPP/PE pair at 160 °C as determined using sPP-EPR block copolymers is close to that reported in the literature for the head-to-head polypropylene-*block*-polyethylene block copolymer, hhPP-PE, with only a slightly different temperature dependence.[19-21]

In this paper, we are concerned with the determination of a phase diagram of sPP-EPR block copolymers. To draw the phase diagrams, we used the calculated mean-field values for the $\chi(T)$, since in the weakly segregated polyolefin systems, fluctuation effects are generally minimized by the large N needed for phase separation. Furthermore, Maurer et al. studied homopolymer blends and block copolymer thermodynamics and concluded that current theories could not account for block copolymer or homopolymer phase behavior based on a single function for χ.[24] They determined the interaction parameter for PE/EPR using various methods. The value derived for χ from block copolymer order–disorder transition temperature measurements

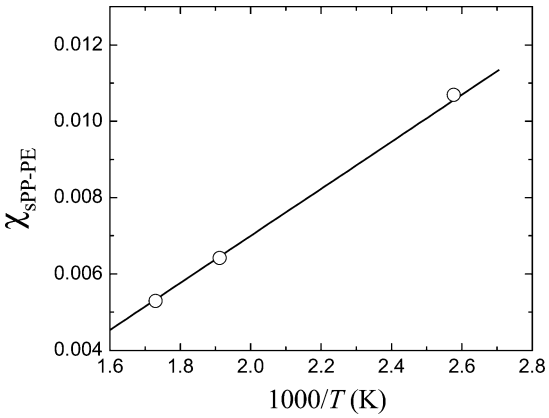

Figure 3. χ_{sPP-PE} values at T_{ODT} as determined using mean-field theory (eq 1). The line represents a fit to the expression $\chi(T) = A/T - B$.

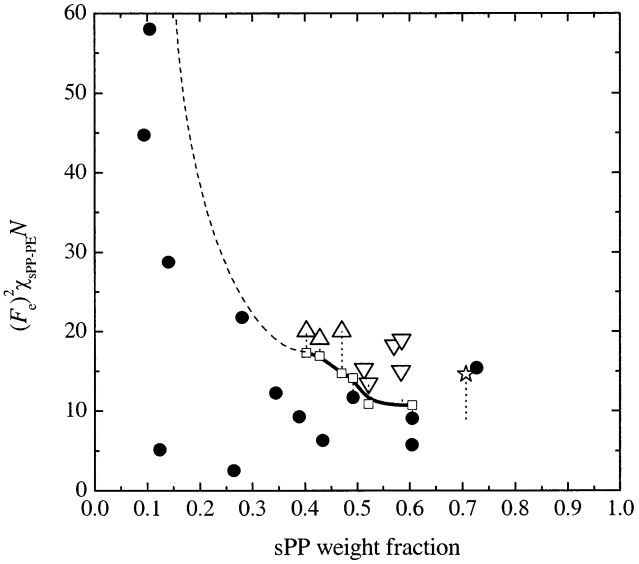

Figure 4. Experimental phase diagram for sPP-EPR diblock copolymers. Each symbol represent a sample of a defined molecular weight and composition. The $(F_e)^2\chi_{sPP-PE}N$ values are calculated at 160 °C using $\chi_{sPP-PE} = 6.2/T - 0.0053$. Solid circles (●) represent disordered melt, triangles (△) identify hexagonal perforated layers (HPL) where the EPR is the majority phase, triangles (▽) are hexagonal perforated layers (HPL′) where sPP is the majority phase, and the open star (☆) represents hexagonally packed EPR cylinders in an sPP matrix. While the composition is given as weight fraction rather than volume fraction of sPP, we believe that these are nearly equal since the melt densities of sPP and EPR should be very similar based on the similarity of the melt densities of sPP and PE.

using the simple mean-field approximation was identical within the experimental error with the $\chi(T)$ results derived from homopolymer blends.

Phase Diagram: Syndiotactic Polypropylene-*block*-poly(ethylene-*co*-propylene) (sPP-EPR). Figure 4 shows the phase diagram for syndiotactic polypropylene-*block*-poly(ethylene-*co*-propylene) diblock copolymer melts. The melt morphology was analyzed using TEM on samples quenched from 160 °C. For a fixed sPP block weight fraction, the phase diagram shows the block copolymer morphology as a function of the degree of segregation, χN. Each symbol in the phase diagram corresponds to a sample of defined molecular weight and composition. The values for the various samples are calculated at 160 °C by using the experimentally determined χ_{sPP-PE} from eq 2, where χ =

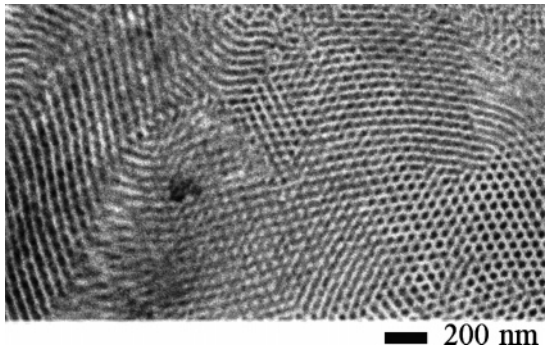

Figure 5. Representative transmission electron micrograph showing a hexagonal perforated layer morphology (HPL′). Weight fraction of sPP is 0.58 (sample PP58.173EPR). Rubbery amorphous EPR domains are stained with RuO_4.

$\chi_{sPP-EPR} = (F_e)^2\chi_{sPP-PE}$. Different symbols corresponding to unique morphologies observed by TEM are explained in the figure caption. The solid line shows the boundary between the ordered and disordered phases as determined by dynamic mechanical rheology. Vertical dotted lines represent the experimental temperature range as studied by rheology, and open squares are the mean-field χN values at the T_{ODT} as calculated from experimentally determined order−disorder transition temperatures.

The phase diagram shows a large number of samples that are classified as hexagonal perforated layer morphologies (HPL or HPL′). In general, the hexagonal perforated layer morphology is metastable in diblock copolymer melts and is typically found in weakly segregated systems (i.e., close to the order−disorder transition). After sufficient long annealing, it normally transforms into the stable equilibrium morphology, usually a lamellar, cylindrical, or gyroid phase. We believe that the hexagonal perforated layer morphologies observed in sPP-EPR block copolymers are also metastable structures. While the results in Figure 4 are for samples quenched from 160 °C, preliminary results also indicate that the melt morphology is preserved even during slow cooling despite the crystallization of the sPP. All the microphase-separated samples have relatively high molecular weights, and therefore the polymer chains are highly entangled, which may hinder the microphase-separated structure from reorganizing during the crystallization process. Because of the large number of entanglements per chain (estimated to be between 25 and 100 depending on M_n), the polymer chain mobility is very low, which may explain why we so frequently observe these metastable morphologies despite our rather long annealing times.

Figures 5−7 show the representative TEM micrographs of different phases observed. Samples are stained using RuO_4, which predominately stains the amorphous regions. Therefore, EPR domains appear black and crystalline sPP domains appear white. Figure 5 shows a clear hexagonal arrangement of dark EPR domains in sample PP58.173EPR. In some regions, hexagonal packing of sPP is also observed. These features are consistent with the hexagonal perforated layer (HPL′) morphology. This morphology is difficult to determine using TEM images alone, and generally both scattering and microscopy data are needed to unambiguously prove the presence of the HPL′ phase. Small-angle X-ray scattering (SAXS) experiments were also attempted, but because of chemical similarity of the sPP and EPR blocks, the electron density contrast for X-ray scattering is negligible. Additionally, because of the large molecular weights of these block copolymers, the scattering is expected to be at very low angles, which are not accessible using our current SAXS apparatus. Neutron scattering using deuterium-labeled samples would overcome these problems, but deuterium labeling may change the phase behavior of this weakly segregated system where the thermodynamics are mainly dominated by weak van der Waals interactions.

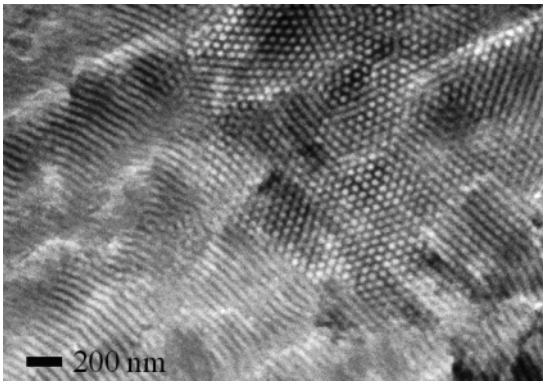

Figure 6. Transmission electron micrograph showing hexagonal perforated layer morphology (HPL). Weight fraction of sPP is 0.47 (PP47.212EPR). Rubbery amorphous EPR domains are stained with RuO_4.

Figure 6 shows the TEM micrograph of the sample PP47.212EPR. The sPP fraction is now 0.47, and a clear sPP hexagonal pattern is observed. Other micrographs show features that are typically observed in samples having layered structures, i.e., regions where layer spacing seems to be larger due to the tilt of the layers viewed in projection. Also, regions with weak contrast of inverse hexagonal packing of EPR domains are observed. This phase is designated as HPL where sPP is a minority phase. However, because of the lack of comprehensive scattering data, we cannot rule out the possibility of having a kinetically frozen coexistence of hexagonal sPP cylindrical and lamellar phases. Despite the long annealing time, we believe that all these observed HPL structures are metastable and equilibrium morphologies are either hexagonal cylinders, lamellar, or bicontinuous gyroid depending on the compositions.

At higher sPP fractions, cylindrical morphologies were also observed. In this composition regime, the amorphous EPR domains are embedded in the crystalline sPP matrix. Figure 7 shows an example of hexagonal cylindrical morphology where the soft EPR domains form cylinders in sPP semicrystalline matrix (sample PP71.232EPR). For this specific sample the order−disorder transition was not detected up to the 300 °C, which was the highest temperature studied experimentally.

Syndiotactic Polypropylene-*block*-polyethylene sPP-PE Block Copolymers. We also used the living catalyst system **1**/MAO to synthesize diblock copolymers with an ethylene fraction of 1.0 in the EPR block, i.e., pure syndiotactic propylene−polyethylene block copolymers. Compared to the sPP-EPR block copolymer systems, the difference lies in the fact that both blocks are crystallizable. Figure 8 shows the preliminary phase diagram for sPP−PE block copolymers obtained following the same procedure described previously. Because of the high ethylene fraction and the large molecular

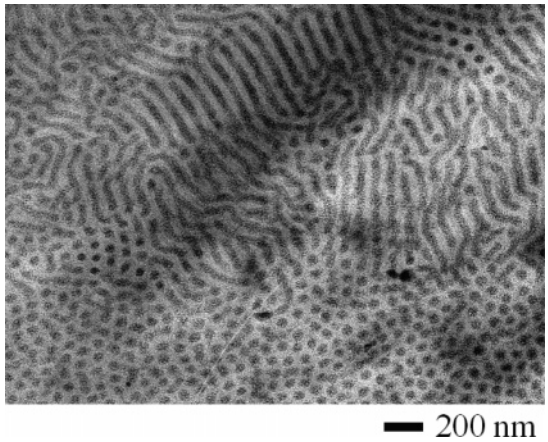

Figure 7. Example of the cylindrical morphology where the dark EPR phase is the minority phase forming hexagonal cylinders embedded in the sPP matrix. Sample PP71.232EPR, with $f_{sPP} = 0.71$.

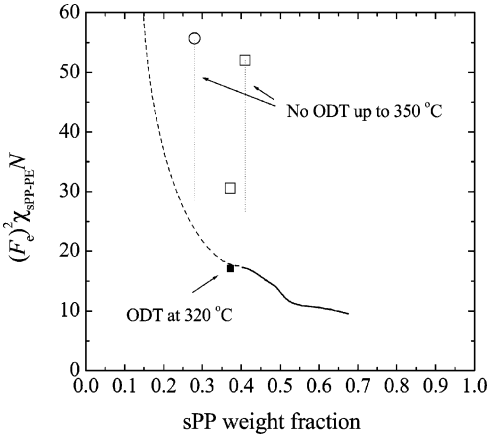

Figure 8. Experimental phase diagram for sPP-PE diblock copolymers. The ethylene fraction is 1.0, and $\chi_{sPP-PE}N$ values are calculated at 160 °C using the $\chi_{sPP-PE} = 6.2/T - 0.0053$ determined experimentally. Squares represent samples with lamellar morphologies while the circle represents a sample with sPP cylinders. Vertical dotted lines represent the experimental temperature range 160−350 °C. Sample PP37.77PE shows an order−disorder transition at 320 °C, and the corresponding mean field χN value is marked by a solid square.

weights, these samples are more strongly segregated compared to sPP-EPR samples. The phase diagram shows only classical morphologies: samples PP37.192PE and PP41.327PE are lamellar, and sample PP28.350PE forms sPP cylinders in the PE matrix. Dotted vertical lines represent the experimentally studied temperature range (160−350 °C), and only the lowest molecular weight sample PP37.192PE shows the order−disorder transition at ~320 °C, which is consistent with our data for the sPP-EPR system. By comparison, the order−disorder transition phase boundary for the sPP-EPR system is marked in Figure 8 by solid and dashed lines. The χN value at the $T_{ODT} = 320$ °C for the sample PP37.192PE is marked in Figure 8 by a solid square.

A typical TEM image of sample PP41.327PE is shown in Figure 9a. The morphology is clearly lamellar where the sPP and PE layers alternate. The higher magnification micrograph in Figure 9b reveals the polyethylene crystal fine structure. Inside the PE layers, approximately 20 nm thick crystalline PE lamellae alternate with amorphous PE domains. Since the RuO_4 stain penetrates more easily into the low-T_g PE amorphous domains, in Figure 9a,b the crystalline polypropylene

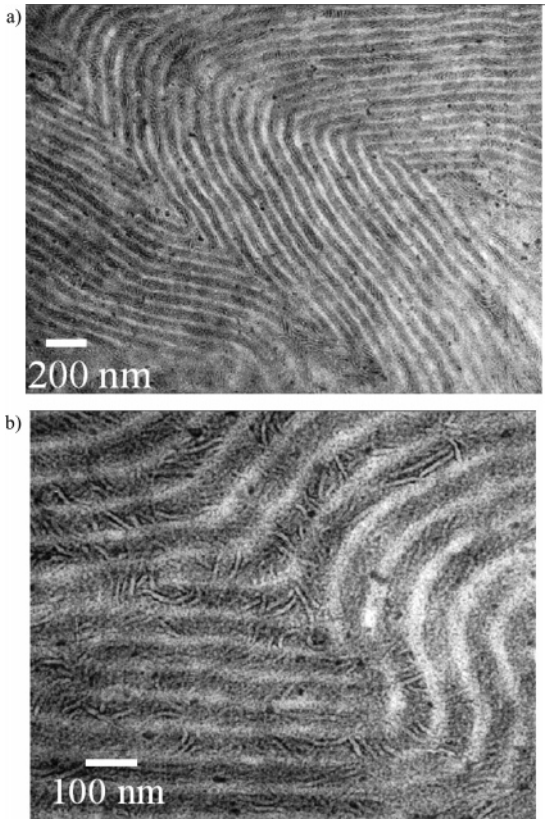

Figure 9. (a) Transmission electron microscopy image of sPP-PE (sample PP41.327PE with $f_{sPP} = 0.41$). Morphology is lamellar, where semicrystalline sPP layers alternate with semicrystalline PE layers. (b) Higher magnification image of same sample. Owing to the selective RuO_4 staining, the partly crystalline sPP layers and PE crystals appear white and the amorphous PE domains are almost black.

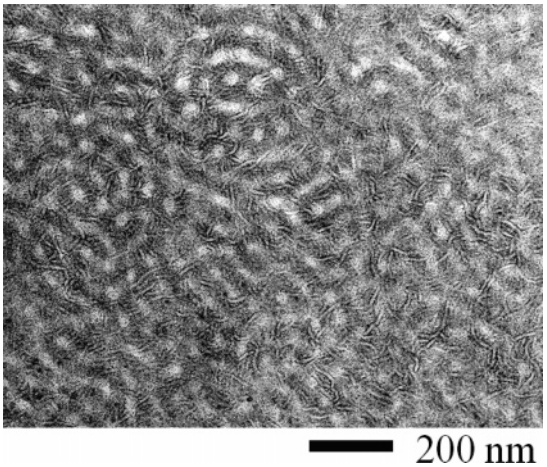

Figure 10. Transmission electron micrograph of sample PP28.350PE with $f_{sPP} = 0.28$. The micrograph reveals a cylindrical morphology where the minority sPP domains form cylinders in the semicrystalline PE matrix.

layers and PE crystals appear white and the amorphous PE is dark. By decreasing the fraction of syndiotactic polypropylene, the lamellar morphology changes to cylindrical, where the polypropylene cylinders are embedded in the semicrystalline polyethylene matrix. Figure 10 shows a typical electron microscopy image of this cylindrical morphology for sPP-PE block copolymers.

Crystallization and Melting. *sPP-EPR Block Copolymers.* The effect of block copolymer microstructure

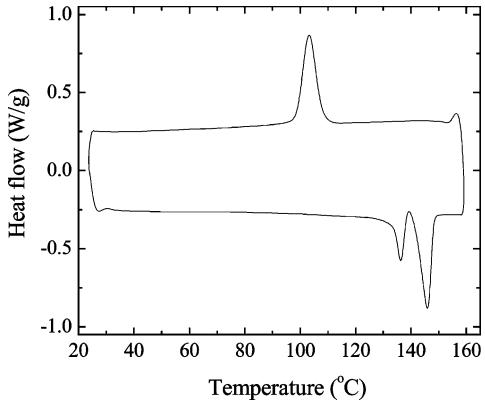

Figure 11. Typical differential scanning calorimetry scans for sPP-EPR block copolymers (sample PP60.74EPR). Data shown are recorded during the second heating and cooling cycle.

on sPP and PE crystallization was investigated using DSC. Figure 11 presents a typical DSC heating/cooling thermogram for the sPP-EPR block copolymer samples. Data are recorded during the second heating/cooling cycle at the rate of 5 °C/min. The DSC curve shows a double melting endotherm, indicating that melting is immediately followed by recrystallization. Similar melting behavior for sPP homopolymers is reported in the literature, and the higher temperature peak of the two is more pronounced at slow heating rates[46,47] These investigators studied sPP homopolymer crystallization and found that the enthalpy of the high-temperature endotherm increases with decreasing heating rate and decreasing crystallization temperature. The lower melting endotherm corresponds to the melting of crystalline aggregates formed as a result of crystallization during cooling and holding at room temperature, whereas the higher temperature endotherm is the result of melting of the crystals that are formed by recrystallization during heating.[46,47] During cooling, sample PP60.74EPR crystallizes at approximately 103 °C, and the corresponding higher temperature endotherm has a peak at a melting temperature of 146 °C, when scanning at the rate of 5 °C/min. Relatively large supercooling of sPP crystallization is observed for all samples, and surprisingly the crystallization temperature is found to be independent of sample melt morphology.

Melting and crystallization temperatures were observed to correlate best with the total molecular weight of block copolymer, a correlation that is shown in Figure 12. For T_m, the peak temperature of the higher temperature endotherm is plotted. A clear linear correlation is found for a large range of the molecular weights studied, between 73 and 580 kg/mol. Nevertheless, no correlation is observed between different morphologies or between the ordered and disordered samples. Melting temperatures correlate very well with the total molecular weight, and almost all samples overlay the least-squares fit line. Only the three highest molecular weight samples deviate slightly from this line. We conclude from this result that the confinement of the crystalline block within nanodomains does not hinder its crystallization or affect the thickness or perfection of the sPP crystals, at least relative to the much larger influence of M_n. Note that in this study a majority of the samples had a morphology where the sPP forms a continuous phase (e.g., HPL′ or EPR hexagonal cylinders), and a truly isolated confinement morphology, such as sPP spheres, was not observed in this work. The depression

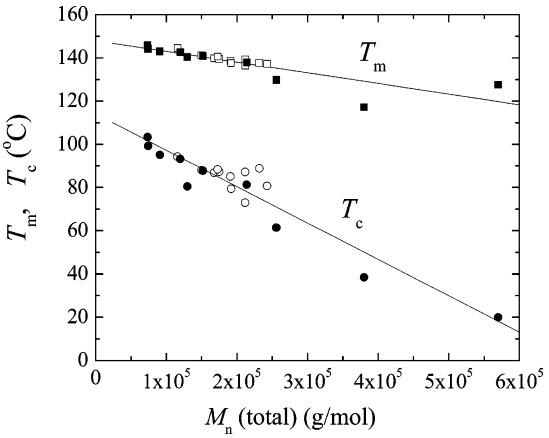

Figure 12. Melting and crystallization temperatures as a function of total block copolymer molecular weight. Samples that are microphase separated at the crystallization temperature are marked with open symbols, and samples that form a homogeneous disordered melt at T_c are marked with filled symbols.

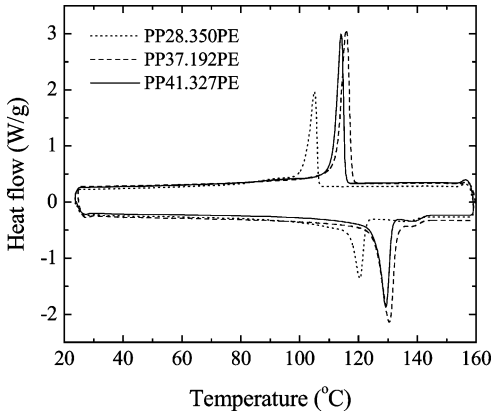

Figure 13. Differential scanning calorimetry scans for the sPP-PE block copolymer samples. Data are recorded during the second heating and cooling cycle at a rate of 5 °C/min.

of T_c for large M_n is likely due to the highly entangled nature of the block copolymer melt, although these effects seem larger for a given molecular weight change than the corresponding changes caused in T_c of homopolymer sPP that can be inferred from the changes in crystallization kinetics with M_n.[48]

sPP-PE Block Copolymers. The nucleation and growth of syndiotactic polypropylene crystals is known to be slow.[31,48,49] Therefore, in sPP-PE block copolymers where both blocks can crystallize, polyethylene domains crystallize first and the heat released from this crystallization tends to obscure the signal from any sPP crystallization during cooling in DSC. During heating, the polyethylene crystals melt at temperatures between 120 and 130 °C, and only a small sPP melting endotherm is observed around 140 °C. Molecular weight has a large effect on the sPP crystallization, but it seems to have only a small influence on the crystallization and melting temperatures of the PE block. This can be seen in Figure 13 by comparing samples PP37.192PE and PP41.327PE, which both have a lamellar morphology and nearly the same composition but differ in molecular weights. The PE melting and crystallization temperatures of the higher molecular weight sample are only 1.2 and 1.7 °C lower, respectively. Comparing the samples PP41.327PE and PP28.350PE, which have similar total molecular weight but different morpholo-

gies, we notice that sample PP28.350PE, whose morphology consists of sPP cylinders in a PE matrix, has polyethylene melting and crystallization temperatures 10 °C lower than those of sample PP41.327PE, whose morphology is lamellar. The morphology of microphase separation seems to influence the PE block crystallization even though it does not affect the crystallization of sPP block.

Summary

Order−disorder transition temperatures of syndiotactic polypropylene-*block*-poly(ethylene-*co*-propylene) diblock copolymers were determined by dynamic mechanical spectroscopy and confirmed by TEM observations. These data were used to determine the temperature-dependent Flory−Huggins interaction parameter $\chi_{sPP-PE} = 6.2/T - 0.0053$ using mean-field theory. The morphologies of the ordered phases of sPP-EPR and sPP-PE diblock copolymers were investigated by TEM. A large number of the ordered sPP-EPR samples exhibit a morphology that is tentatively identified as a hexagonal perforated layer morphology (HPL or HPL′). While this phase is predicted to be metastable, it persists for such long annealing times that it is impossible to establish what the equilibrium morphology really is. All samples had relatively high molecular weights, and therefore polymer chains were highly entangled, which may explain why these metastable morphologies still persist despite the rather long annealing times.

The effect of block copolymer microstructure on sPP and PE crystallization was studied using differential scanning calorimetry. In the case of syndiotactic polypropylene-*block*-poly(ethylene-*co*-propylene) block copolymers, the DSC curves show a double melting endotherm indicating that melting is immediately followed by recrystallization. When crystallized at a cooling rate of 5 °C/min, a relatively large supercooling of sPP crystallization is observed for all sPP-EPR block copolymers, and surprisingly the crystallization temperature is found to be independent of sample melt morphology. The sPP melting and crystallization temperatures were discovered to correlate best with the sPP-EPR block copolymer total molecular weight, with higher molecular weights producing lower T_c and T_m. We conclude that the confinement of the sPP crystalline block within nanodomains does not significantly hinder sPP crystallization. Preliminary results however indicate that the block copolymer nanodomain confinement has an effect on polyethylene crystallization in the sPP-PE block copolymers. Polyethylene crystallization temperatures were higher for a lamellar morphology in comparison to a morphology where sPP cylinders were embedded in a polyethylene matrix.

Acknowledgment. This work was supported by the Mitsubishi Chemical Center for Advanced Materials MC-CAM. This work made use of UCSB-MRL Central Facilities supported by the National Science Foundation under Award DMR00-80034. G.W.C. gratefully acknowledges a Packard Foundation Fellowship in Science and Engineering and the Cornell Center for Materials Research, supported through the NSF MRSEC program (DMR-0079992).

References and Notes

(1) Vasile, C., Ed. *Handbook of Polyolefins*, 2nd ed.; Marcel Dekker: New York, 2000.
(2) Boor, J. J. *Ziegler−Natta Catalysts and Polymerizations*; Academic: New York, 1979.
(3) Brintzinger, H. H.; Fischer, D.; Muelhaupt, R.; Rieger, B.; Waymouth, R. M. *Angew. Chem., Int. Ed. Engl.* **1995**, *34*, 1143−70.
(4) Ewen, J. A. *J. Am. Chem. Soc.* **1984**, *106*, 6355−64.
(5) Kaminsky, W.; Kuelper, K.; Brintzinger, H. H.; Wild, F. R. W. P. *Angew. Chem.* **1985**, *97*, 507−8.
(6) Resconi, L.; Cavallo, L.; Fait, A.; Piemontesi, F. *Chem. Rev.* **2000**, *100*, 1253−1345.
(7) Coates, G. W.; Waymouth, R. M. *Science* **1995**, *267*, 217−19.
(8) For leading references on stopped-flow techniques for block copolymer synthesis, see: (a) Liu, B.; Matsuoka, H.; Terano, M. *Macromol. Rapid Commun.* **2001**, *22*, 1−24. (b) Mori, H.; Yamahiro, M.; Tashino, K.; Ohnishi, K.; Nitta, K.; Terano, M. *Macromol. Rapid Commun.* **1995**, *16*, 247−52.
(9) Coates, G. W.; Hustad, P. D.; Reinartz, S. *Angew. Chem., Int. Ed.* **2002**, *41*, 2236−2257.
(10) Tian, J.; Hustad, P. D.; Coates, G. W. *J. Am. Chem. Soc.* **2001**, *123*, 5134−5135.
(11) Mason, A. F.; Tian, J.; Hustad, P. D.; Lobkovsky, E. B.; Coates, G. W. *Isr. J. Chem.* **2003**, *42*, 301−306.
(12) For synthesis of alternating and multiblock copolymers from ethylene and cyclopentene, see: Fujita, M.; Coates, G. W. *Macromolecules* **2002**, *35*, 9640−9647.
(13) For the living insertion/isomerization polymerization of 1,5-hexadiene and synthesis of related 3-vinylene tetramethylene containing block copolymers, see: Hustad, P. D.; Coates, G. W. *J. Am. Chem. Soc.* **2002**, *124*, 11578−11579. For further synthesis and cross-metathesis functionalization of these polymers, see: Mathers, R. T.; Coates, G. W. *Chem. Commun.* **2004**, 422−423.
(14) For a review, see: Makio, H.; Kashiwa, N.; Fujita, T. *Adv. Synth. Catal.* **2002**, *344*, 477−493.
(15) (a) Mitani, M.; Nakano, T.; Fujita, T. *Chem.—Eur. J.* **2003**, *9*, 2396−2403. (b) Mitani, M.; Furuyama, R.; Mohri, J.; Saito, J.; Ishii, S.; Terao, H.; Nakano, T.; Tanaka, H.; Fujita, T. *J. Am. Chem. Soc.* **2003**, *125*, 4293−4305. (c) Ono, S. S.; Matsugi, T.; Matsuoka, O.; Kojoh, S.-i.; Fujita, T.; Kashiwa, N.; Yamamoto, S. *Chem. Lett.* **2003**, *32*, 1182−1183. (d) Mitani, M.; Mohri, J.; Yoshida, Y.; Saito, J.; Ishii, S.; Tsuru, K.; Matsui, S.; Furuyama, R.; Nakano, T.; Tanaka, H.; Kojoh, S.-i.; Matsugi, T.; Kashiwa, N.; Fujita, T. *J. Am. Chem. Soc.* **2002**, *124*, 3327−3336. (e) Mitani, M.; Furuyama, R.; Mohri, J.-I.; Saito, J.; Ishii, S.; Terao, H.; Kashiwa, N.; Fujita, T. *J. Am. Chem. Soc.* **2002**, *124*, 7888−7889. (f) Saito, J.; Mitani, M.; Mohri, J.-I.; Yoshida, Y.; Matsui, S.; Ishii, S.-I.; Kojoh, S.-I.; Kashiwa, N.; Fujita, T. *Angew. Chem., Int. Ed.* **2001**, *40*, 2918−2920. (g) Saito, J.; Mitani, M.; Mohri, J.-I.; Ishii, S.-I.; Yoshida, Y.; Matsugi, T.; Kojoh, S.-I.; Kashiwa, N.; Fujita, T. *Chem. Lett.* **2001**, 576−577. (h) Kojoh, S.-I.; Matsugi, T.; Saito, J.; Mitani, M.; Fujita, T.; Kashiwa, N. *Chem. Lett.* **2001**, 822−823.
(16) Busico, V.; Cipullo, R.; Friederichs, N.; Ronca, S.; Togrou, M. *Macromolecules* **2003**, *36*, 3806−3808.
(17) Tshuva, E. Y.; Goldberg, I.; Kol, M. *J. Am. Chem. Soc.* **2000**, *122*, 10706−10707.
(18) Hong, S.; Bushelman, A. A.; MacKnight, W. J.; Gido, S. P.; Lohse, D. J.; Fetters, L. J. *Polymer* **2001**, *42*, 5909−5914.
(19) Jeon, H. S.; Lee, J. H.; Balsara, N. P.; Newstein, M. C. *Macromolecules* **1998**, *31*, 3340−3352.
(20) Jeon, H. S.; Lee, J. H.; Balsara, N. P. *Macromolecules* **1998**, *31*, 3328−3339.
(21) Rangarajan, P.; Register, R. A.; Fetters, L. J.; Bras, W.; Naylor, S.; Ryan, A. J. *Macromolecules* **1995**, *28*, 4932−8.
(22) Khandpur, A. K.; Macosko, C. W.; Bates, F. S. *J. Polym. Sci., Part B: Polym. Phys.* **1995**, *33*, 247−52.
(23) Rangarajan, P.; Register, R. A.; Fetters, L. J. *Macromolecules* **1993**, *26*, 4640−5.
(24) Maurer, W. W.; Bates, F. S.; Lodge, T. P.; Almdal, K.; Mortensen, K.; Fredrickson, G. H. *J. Chem. Phys.* **1998**, *108*, 2989−3000.
(25) Zhao, J.; Majumdar, B.; Schulz, M. F.; Bates, F. S.; Almdal, K.; Mortensen, K.; Hajduk, D. A.; Gruner, S. M. *Macromolecules* **1996**, *29*, 1204−15.
(26) Rosedale, J. H.; Bates, F. S.; Almdal, K.; Mortensen, K.; Wignall, G. D. *Macromolecules* **1995**, *28*, 1429−43.
(27) Bates, F. S.; Schulz, M. F.; Rosedale, J. H.; Almdal, K. *Macromolecules* **1992**, *25*, 5547−50.
(28) Hamley, I. W.; Fairclough, J. P. A.; Bates, F. S.; Ryan, A. J. *Polymer* **1998**, *39*, 1429−1437.

(29) Hamley, I. W.; Fairclough, J. P. A.; Terrill, N. J.; Ryan, A. J.; Lipic, P. M.; Bates, F. S.; Towns-Andrews, E. *Macromolecules* **1996**, *29*, 8835−8843.
(30) Ryan, A. J.; Hamley, I. W.; Bras, W.; Bates, F. S. *Macromolecules* **1995**, *28*, 3860−8.
(31) Rangarajan, P.; Register, R. A.; Adamson, D. H.; Fetters, L. J.; Bras, W.; Naylor, S.; Ryan, A. J. *Macromolecules* **1995**, *28*, 1422−8.
(32) Brown, G. M.; Butler, J. H. *Polymer* **1997**, *38*, 3936−3945.
(33) Fetters, L. J.; Lohse, D. J.; Richter, D.; Witten, T. A.; Zirkel, A. *Macromolecules* **1994**, *27*, 4639−47.
(34) Cochran, E. W.; Bates, F. S. *Macromolecules* **2002**, *35*, 7368−7374.
(35) Jones, T. D.; Chaffin, K. A.; Bates, F. S.; Annis, B. K.; Hagaman, E. W.; Kim, M.-H.; Wignall, G. D.; Fan, W.; Waymouth, R. *Macromolecules* **2002**, *35*, 5061−5068.
(36) Fetters, L. J.; Lohse, D. J.; Graessley, W. W. *J. Polym. Sci., Part B: Polym. Phys.* **1999**, *37*, 1023−1033.
(37) Dai, K. H.; Kramer, E. J. *Polymer* **1994**, *35*, 157−61.
(38) Fredrickson, G. H.; Bates, F. S. *Annu. Rev. Mater. Sci.* **1996**, *26*, 501−550.
(39) Ferry, J. D. *Viscoelastic Properties of Polymers*, 3rd ed.; Wiley: New York, 1980.
(40) Han, C. D.; Kim, J.; Kim, J. K. *Macromolecules* **1989**, *22*, 383−94.
(41) Han, C. D.; Kim, J. *J. Polym. Sci., Part B: Polym. Phys.* **1987**, *25*, 1741−64.
(42) Rosedale, J.; Bates, F. S. *Macromolecules* **1990**, *29*, 2329.
(43) Kambour, R. P.; Bendler, J. T.; Bopp, R. C. *Macromolecules* **1983**, *16*, 753.
(44) ten Brinke, G.; Karasz, F. E.; MacKnight, W. J. *Macromolecules* **1983**, *16*, 1827.
(45) Gehlsen, M. D.; Rosedale, J. H.; Bates, F. S.; Wignall, G. D.; Hansen, L.; Almdal, K. *Phys. Rev. Lett.* **1992**, *68*, 2452.
(46) Schmidtke, J.; Strobl, G.; Thurn-Albrecht, T. *Macromolecules* **1997**, *30*, 5804−5821.
(47) Supaphol, P.; Spruiell, J. E. *J. Appl. Polym. Sci.* **2000**, *75*, 44−59.
(48) Rodriquez-Arnold, J.; Zhang, A.; Cheng, S. Z. D.; Lovinger, A. J.; Hsieh, E. T.; Chu, P.; Johnson, T. W.; Honnell, K. G.; Geerts, R. G.; Palackal, S. J.; Hawley, G. R.; Welch, M. B. *Polymer* **1994**, *35*, 1884.
(49) Rodriquez-Arnold, J.; Blu, Z.; Cheng, S. Z. D.; Lovinger, A. J.; Hsieh, E. T.; Johnson, T. W.; Geerts, R. G.; Palackal, S. J.; Hawley, G. R.; Welch, M. B. *Polymer* **1994**, *35*, 5194.

MA0494479